

Deprotonated sulfamic acid and its homodimers: Does sulfamic acid adopt zwitterion during cluster growth?

Zhubin Hu,^{1#} Qiaoqiao Shao,^{1#} Zhipeng Li,^{1,2} Zhenrong Sun,^{1,*} Xue-Bin Wang,^{2,*} and

Haitao Sun^{1,3,4*}

¹ State Key Laboratory of Precision Spectroscopy, School of Physics and Electronic Science, East China Normal University, Shanghai 200241, China

² Physical Sciences Division, Pacific Northwest National Laboratory, 902 Battelle Boulevard, P.O. Box 999, Richland, Washington 99352, USA

³ Collaborative Innovation Center of Extreme Optics, Shanxi University, Taiyuan, Shanxi 030006, China

⁴ NYU-ECNU Center for Computational Chemistry at NYU Shanghai, Shanghai, 200062, China

[#]Z. Hu and Q. Shao contributed equally to this work.

*Corresponding author: htsun@phy.ecnu.edu.cn (H.S); xuebin.wang@pnnl.gov (X.-B.W.); zrsun@phy.ecnu.edu.cn (Z.R.S.).

This is the author's peer reviewed, accepted manuscript. However, the online version of record will be different from this version once it has been copyedited and typeset.
PLEASE CITE THIS ARTICLE AS DOI: 10.1063/5.0190757

Abstract

We present a joint experimental and computational study on the geometric and electronic structures of deprotonated sulfamic acid (SA) clusters $[(SA)_n-H]^-$ ($n = 1,2$) employing negative ion photoelectron spectroscopy (NIPES) and high-level ab initio calculations. The photoelectron spectra produces the vertical/adiabatic detachment energy (VDE/ADE) of the sulfamate anion (SM^-) $H_2N \cdot SO_3^-$ at 4.85 ± 0.05 eV and 4.58 ± 0.08 eV, respectively, and the VDE and ADE of $SM^- \cdot SA$ dimer at 6.41 ± 0.05 eV and 5.87 ± 0.08 eV, respectively. The significantly increased electron binding energies of the dimer confirm the enhanced electronic stability upon the addition of one SA molecule. The CCSD(T)-predicted VDEs/ADEs agree excellently with the experimental data, confirming the identified structures as the most stable ones. Two types of dimer isomers possessing different hydrogen bonding (HB) motifs are identified, corresponding to SM^- binding to a zwitterionic SA ($SM^- \cdot SA_z$) and to a canonical SA ($SM^- \cdot SA_c$), respectively. Two N-H \cdots O HBs and one superior O-H \cdots O HB are formed in the lowest-lying $SM^- \cdot SA_c$, while $SM^- \cdot SA_z$ has three moderate N-H \cdots O HBs, with the former being 4.71 kcal/mol more stable. Further theoretical analyses reveal that the binding strength advantage of $SM^- \cdot SA_c$ over $SM^- \cdot SA_z$ arises from its significant contributions of orbital interactions between fragments, illustrating that sulfamate strongly interacts with its parent SA acid, and preferably chooses the canonical SA in the subsequent cluster formations. Given the prominent presence of SA, this study provides the first evidence that the canonical dimer model of sulfamic acid should exist as a superior configuration during cluster growth.

This is the author's peer reviewed, accepted manuscript. However, the online version of record will be different from this version once it has been copyedited and typeset.

PLEASE CITE THIS ARTICLE AS DOI: 10.1063/5.0190757

I. INTRODUCTION

Sulfamic Acid ($\text{H}_2\text{N}\cdot\text{SO}_3\text{H}$ or $\text{H}_3\text{N}\cdot\text{SO}_3$, SA) is an important inorganic acid with broad applications in industrial syntheses,^{1,2} food chemistry,³ and pharmacology.^{4,5} For example, the substituted sulfamates possessing specific biological activities are exploited for designing various therapeutic agents such as synthetases inhibitors, anti-viral and anti-cancer drugs.^{5,6} SA has been demonstrated to undergo polymerization, forming clusters that contribute to atmospheric nucleation and condensation processes.⁷⁻⁹ Typically, SA contains two structural forms, i.e., the zwitterionic form $^+\text{H}_3\text{N}\cdot\text{SO}_3^-$ (SA_z) and canonical neutral form $\text{H}_2\text{N}\cdot\text{SO}_2\text{OH}$ (SA_c),¹⁰⁻¹⁴ for which the controversy over their stability still exists. Ab initio quantum chemical calculation has revealed that the relative energies of SA_z and SA_c in the gas phase are in close proximity (the latter being slightly lower), and the isomeric conversion necessitates surmounting an energy barrier of 28.6 kcal/mol at the MP2/6-31+G(2d,p) level.¹³ The structural configurations and dipole moments of the SA containing complexes exhibited notable disparities between the gas phase and crystalline state, indicating that the actual geometry of SA is sensitive to its surrounding environment.^{15,16} Moreover, the existence of two isomeric forms of SA introduces additional uncertainty during the growth of SA clusters due to their distinct ability to form multiple hydrogen bond (HB) binding motifs. As a result, the initial SA nucleation may encompass a range of polymerization modalities to optimize the stabilization energy and to reduce the nucleation free energy barriers for particle growth in the atmosphere.

Previous studies on atmospherically relevant clusters that involve SA, sulfuric acid and bisulfate anion have been reported using electrospray ionization (ESI)-mass spectroscopy,^{17,18} infrared photodissociation spectroscopy,¹⁹ and collision-induced dissociation spectroscopy,²⁰ providing valuable speciation and structure information. However, limited information regarding the energetics of the cluster growth can be obtained. To the best of our knowledge, a detailed characterization of geometric, electronic structures and energetics of small SA clusters has not been investigated. More importantly, whether SA adopts zwitterion or canonical form during the cluster growth, a scenario largely dictated by optimizing intermolecular noncovalent interactions (NCI), remains an interesting open question. Gas-phase negative ion photoelectron spectroscopy (NIPES) has been demonstrated as a powerful and robust technique to obtain the geometric, energetic, and electronic structure information for molecular ion clusters that can be size-selected

composition-tailored to serve as ideal models for probing and untangling often complex NCIs important to the formation of critical nucleation embryos.^{21, 22}

In this work, we combine NIPES and ab initio quantum chemical calculations to study the geometric and electronic structures of deprotonated SA anionic clusters, including the sulfamate anion $\text{H}_2\text{N}\cdot\text{SO}_3^-$ (SM^-) and its complex with one SA molecule. Notably, we present direct evidence that the canonical form of SA is favored over its zwitterion to interact with SM^- , suggesting this type of dimer $\text{SM}^- \cdot \text{SA}_c$ to be dominant during the cluster growth. Detailed structural, bonding, and energy characterizations are further performed to highlight the advantage of this type of HB binding motif in enhancing the stability of the SA dimer.

II. Experimental details

The experiments were carried out using a magnetic-bottle NIPES apparatus equipped with an ESI source, a quadruple mass spectrometer (QMS), a temperature-controlled cryogenic ion trap, and a time-of-flight (TOF) mass spectrometer.^{21, 23} The spraying solution of 0.1 mM was prepared by dissolving SA in a mixed solvent of water and methanol at ratio of 1:3 in a N_2 glove box. The deprotonated SA anionic clusters $[(\text{SA})_n\text{-H}]^-$ ($n = 1\text{-}5$), generated by the ESI source, were first detected by QMS, then deflected by a 90° ion bender into the three-dimensional cryogenic ion trap, where the anions were accumulated and cooled to 20 K via collisions with a buffer gas (20% H_2/He) for 20-100 ms. After cooling, the anions were pulsed out, mass-to-charge selected, and subsequently decelerated, before photodetached with a 157 nm (7.886 eV) laser beam from a F_2 excimer laser. Only the monomer ($n = 1$) and dimer ($n = 2$) spectra were obtained because the electron binding energies (EBEs) of the larger clusters ($n > 2$) approach or exceed the photon energy limit. The detached photoelectrons were collected with nearly 100% efficiency by the magnetic bottle and analyzed in a 5.2 m long electron flight tube. The laser was operated at 20 Hz with the ion beam off and on at alternating laser shots, affording shot-to-shot background subtraction. The obtained TOF electron spectra were converted to the electron kinetic energy spectra, calibrated with the known spectra of I^- and $\text{Au}(\text{CN})_2^-$.^{24, 25} The EBE spectra were obtained by subtracting the electron kinetic energy spectra from the detached photon energy. The energy resolution ($\Delta E/E$) was $\sim 2\%$, *i.e.*, ~ 20 meV full width at half-maximum (FWHM) for 1 eV kinetic energy electrons.

This is the author's peer reviewed, accepted manuscript. However, the online version of record will be different from this version once it has been copyedited and typeset.

PLEASE CITE THIS ARTICLE AS DOI: 10.1063/5.0190757

III. Computational methodology

Scheme S1 in the Supplementary Material outlines the workflow to search the lowest-lying structures of the deprotonated sulfamic acid dimer clusters. First, roughly 10000 initial configurations were randomly constructed for the dimer using the Molclus²⁶ code, followed by an initial geometry optimization at the semi-empirical PM6-D3H4²⁷ level using the MOPAC²⁸ program. They were refined in the second-round optimization at the density functional theory (DFT)-B3LYP^{29, 30}-D3(BJ)³¹/6-31+G(d, p) level to select dozens of the low-lying isomers with their relative energies < 10 kcal/mol. Further, these isomer candidates were fully optimized at the DFT-B3LYP-D3(BJ) level using a sufficiently large aug-cc-pVTZ³² basis set, and were sorted out in an order according to their relative energies. Harmonic vibrational frequency analyses were carried out at the same level to ensure the stability of these geometries. Single-point (SP) energies of the anions and corresponding ionized neutrals were calculated at the high-level coupled-cluster CCSD(T)³³/aug-cc-pVTZ level. The theoretical vertical detachment energies (VDEs) and adiabatic detachment energies (ADEs) (including zero-point energy (ZPE) corrections) were calculated by the energy differences between the corresponding neutrals and anions, with the former based on the fixed anion geometries, while the latter based on their respective optimized geometries. The binding energy (BE) of the dimer was calculated by the energy difference between the dimer and the sum of fragments using counterpoise method of Boys and Bernardi³⁴ with the basis set superposition error (BSSE) correction. The Laplacian bond order (LBO)³⁵, charge of natural population analysis (NPA) and extended transition state-natural orbitals for chemical valence (ETS-NOCV)³⁶ analysis were conducted using the Multiwfn code.³⁷ The energy decomposition analysis (EDA) of HBs in the anionic dimers were carried out by the symmetry adapted perturbation theory (SAPT)³⁸ at the SAPT2+(3) δ MP2/aug-cc-pVTZ level using the Psi4 package,³⁹ and dispersion-corrected DFT method at the B3LYP-D3(BJ)/6-311+G(2d,p) level using sobEDAw code,⁴⁰ respectively. All the DFT and coupled-cluster calculations were performed with the Gaussian 16 software.⁴¹

This is the author's peer reviewed, accepted manuscript. However, the online version of record will be different from this version once it has been copyedited and typeset.
PLEASE CITE THIS ARTICLE AS DOI: 10.1063/5.0190757

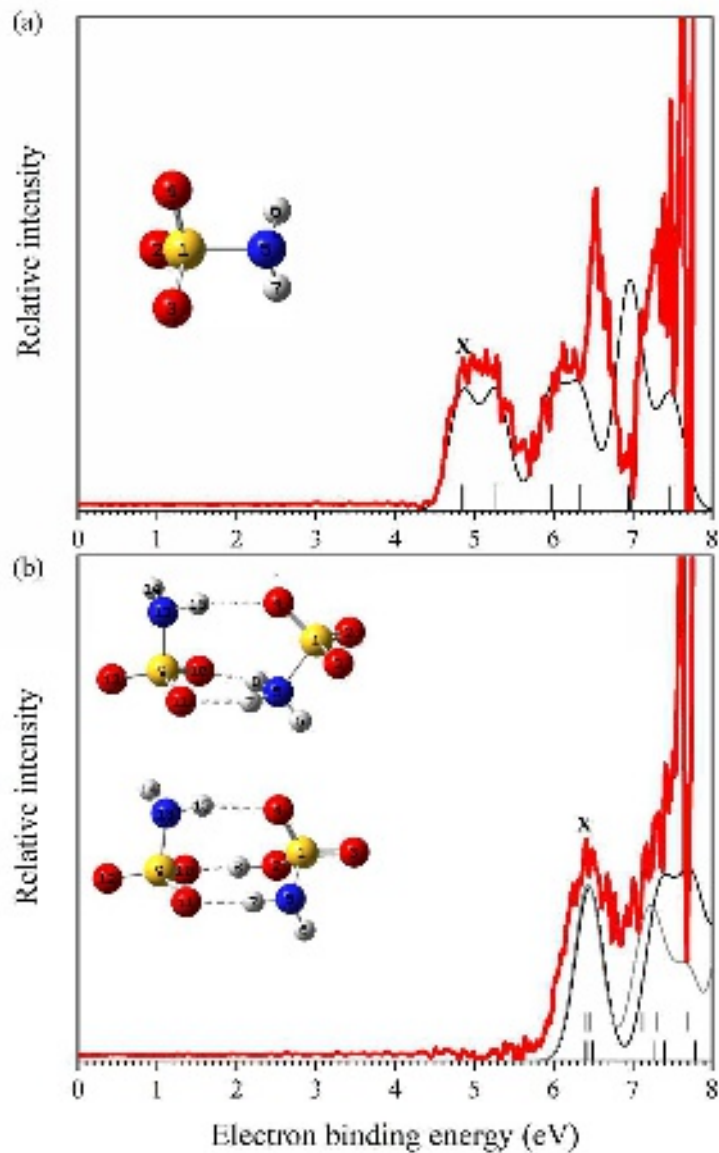


FIG. 1. Cryogenic 157 nm NIPE spectra (red curves) of the deprotonated sulfamic acid (SA) monomer, i.e., sulfamate anion $\text{H}_2\text{N}\cdot\text{SO}_3^-$ (SM^-) (a) and the dimer $[(\text{SA})_2 - \text{H}]^-$ (b). The density of state (DOS) spectra was simulated using a gaussian with a 0.40 eV FWHM for each state and the HOMO level shifted to match the experimental VDE (black curves and bars denote the spectra for SM^- , $\text{SM}^- \cdot \text{SA}_c$ and their corresponding frontier occupied molecular orbitals, respectively, while the grey ones for $\text{SM}^- \cdot \text{SA}_z$).

IV. Negative ion photoelectron spectroscopy (NIPES)

This is the author's peer reviewed, accepted manuscript. However, the online version of record will be different from this version once it has been copyedited and typeset.

PLEASE CITE THIS ARTICLE AS DOI: 10.1063/5.0190757

The cryogenic 20 K 157 nm NIPE spectra of the deprotonated SA monomer and dimer $[(SA)_n - H]^-$ ($n = 1, 2$) are shown in Fig. 1. The lowest band in each spectrum, peak X, represents the transition from the ground state of the anion to the ground state of the corresponding neutral. The experimental VDE is determined from the maximum of peak X, while ADE is estimated as the sum of the instrumental resolution and the EBE at the crossing point of the onset of peak X and the EBE axis. The measured VDE and ADE are 4.85 and 4.58 eV for the deprotonated SA monomer (i.e., SM^-), while 6.41 and 5.87 eV for the dimer (i.e., $SM^- \cdot SA$), respectively (Table I). Upon complexing with one SA molecule, the EBE of SM^- is significantly blue-shifted by ~ 1.56 eV for VDE and ~ 1.29 eV for ADE, indicating that the intermolecular binding interactions between SM^- and SA greatly enhance the electronic stability of the dimer complex. Typically, the VDE difference (ΔVDE) between the dimer and monomer can be used to evaluate the intermolecular interaction strength in the dimer.^{21, 42} The ΔVDE of 1.56 eV obtained here suggest a binding strength comparable to those (1.3 \sim 1.8 eV) of bisulfate (HSO_4^-) and succinate ($HO_2C(CH_2)_2CO_2^-$) interacting with organic acids.^{22, 43} The difference between VDE and ADE, $|VDE - ADE|$, gauges the rising steepness of the first band. The $|VDE - ADE|$ values for the monomer and dimer are 0.27 and 0.54 eV, respectively, suggesting a relatively larger geometry distortion upon photodetaching for the dimer or the possible coexistence of multiple low-lying isomers in the experiment. It should be noted that the dimer can possess two possible isomers including the zwitterionic or canonical form of SA, i.e., $SM^- \cdot SA_z$ or $SM^- \cdot SA_c$, respectively. Given this, it remains a challenge to assign the molecular structures of the dimer cluster from the experimental perspective alone and high-level ab initio calculations are thus performed to assist in identifying the lowest lying (most stable) isomers.

TABLE I. Experimental and calculated VDEs and ADEs (in eV) of the deprotonated SA monomer (SM^-), dimers ($SM^- \cdot SA_z$, $SM^- \cdot SA_c$), and their BEs (in kcal/mol).

	VDE (eV)		ADE (eV)		BE (kcal/mol) ^b
	Expt.	Calc. ^a	Expt.	Calc. ^a	
SM^-	4.85 ± 0.05	4.89	4.58 ± 0.08	4.53	-
$SM^- \cdot SA_z$	6.41 ± 0.05	6.37	5.87 ± 0.08	5.31	43.84
$SM^- \cdot SA_c$	6.41 ± 0.05	6.40	5.87 ± 0.08	5.65	48.79

^a Based on the lowest structure of each type; ^b Calculated using the counterpoise method at the CCSD(T)/aug-cc-pVTZ level.

V. Theoretical results and discussion

A. Optimized geometries

Fig. 2 shows the lowest optimized structures for SA in both zwitterionic (SA_z) and canonical (SA_c) forms, the deprotonated anion SM^- and its corresponding ionized neutral SM^* , various SA homodimer clusters, i.e., $SM^- \cdot SA_z$, $SM^- \cdot SA_c$ and their corresponding photodetached neutrals $SM^* \cdot SA_z$, $SM^* \cdot SA_c$ as well as $SA_z \cdot SA_z$, $SA_z \cdot SA_c$. As seen in Fig. S1, the canonical SA_c is 1.58 kcal/mol more stable than its zwitterionic counterpart SA_z at the CCSD(T)/aug-cc-pVTZ level. The Laplacian bond order (LBO), a useful index to define the strength of covalent interactions, is thus computed to characterize the degree of covalency in S-N bond (Figure S2). The calculated small LBO of 0.139 (bond length of 2.07 Å) in SA_z confirms its zwitterionic character, while the LBO of 0.928 (bond length of 1.65 Å) in SA_c suggests an apparent covalent bond. The lowest-lying isomer of SM^- has a mirror symmetric configuration and its S-N bond length (1.75 Å) lies between the two SA forms with a moderate LBO of 0.618. After photodetaching one extra electron, the S-N bond length in SM^* is shortened to 1.65 Å and the resulting LBO increases to 0.935, suggesting a significant increase in covalency. The distinct LBO values for the S-N bond in different forms of the monomer such as SA_z (0.139), SA_c (0.928), SM^- (0.618) and SM^* (0.935) confirm that the specific configuration of SA is sensitive to its surrounding environments.¹³ Meanwhile, upon photodetachment of SM^- , the relative position of SO_3 and NH_2 moieties rotates anticlockwise with the dihedral angle of ${}^4O-{}^1S-{}^5N-{}^6H$ by $\sim 30^\circ$.

This is the author's peer reviewed, accepted manuscript. However, the online version of record will be different from this version once it has been copyedited and typeset.
PLEASE CITE THIS ARTICLE AS DOI: 10.1063/5.0190757

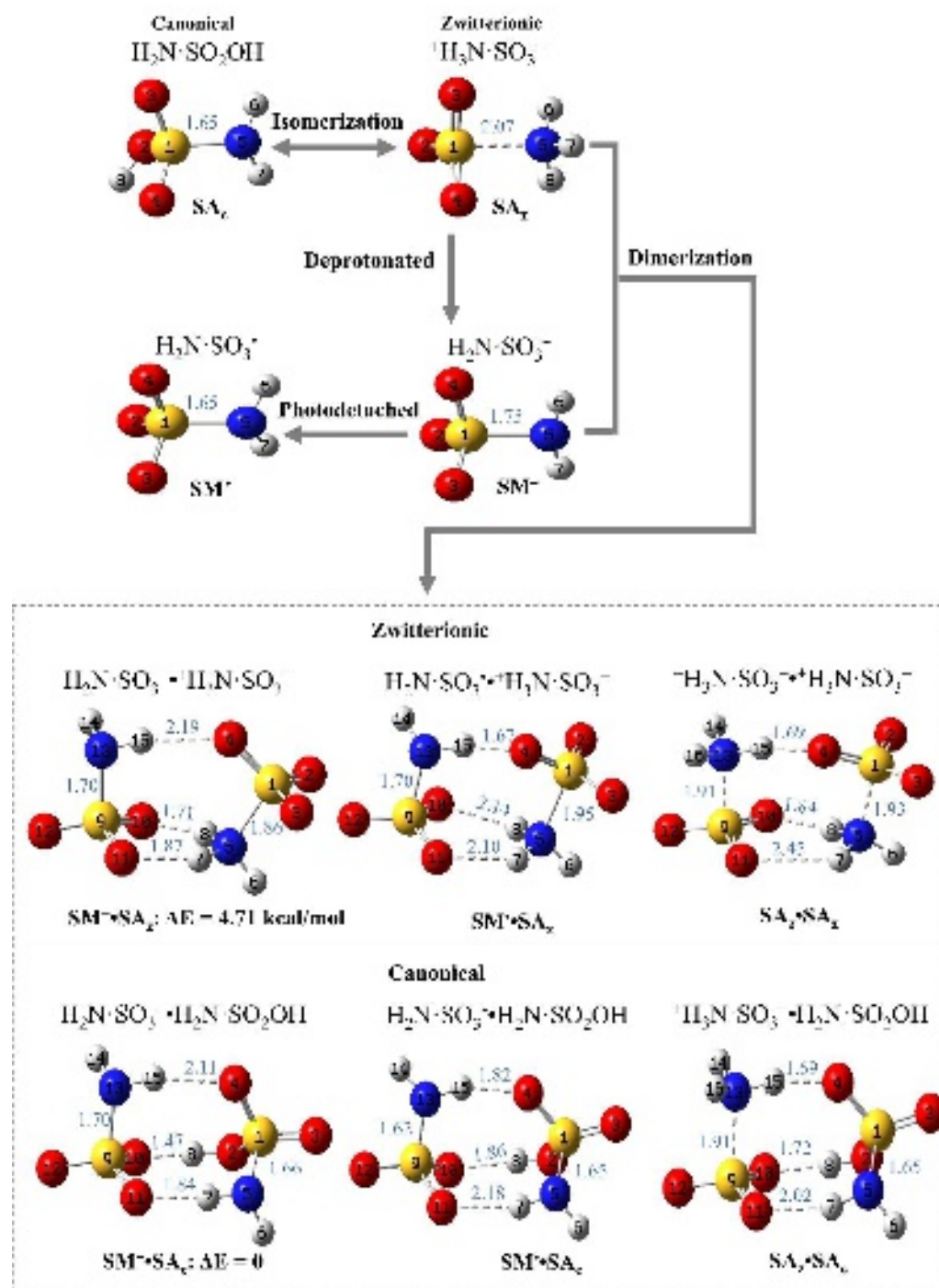


FIG. 2. The lowest-lying B3LYP-D3(BJ)/aug-cc-pVTZ geometries of the monomer SA_z, SA_c, its deprotonated anion SM⁻ and ionized neutral SM⁺, various types of the dimer clusters SM⁻•SA_z/SM⁺•SA_z, SM⁻•SA_c/SM⁺•SA_c, SA_z•SA_z and SA_z•SA_c. The red, yellow, blue, and white balls represent the O, S, N, and H atoms, respectively. The S-N bond lengths and HB lengths (in Å) are also listed in light blue.

The deprotonated homodimer clusters have two types of isomers, i.e., SM^- complexing with zwitterionic or canonical SA, denoted as $\text{SM}^- \cdot \text{SA}_z\text{-x}$ and $\text{SM}^- \cdot \text{SA}_c\text{-x}$, respectively, with the extension $x = a, b, c, \dots$ standing for distinct isomeric structures in the order of increasing energy. The lowest-lying isomer of each type of $\text{SM}^- \cdot \text{SA}_z\text{-a}$ and $\text{SM}^- \cdot \text{SA}_c\text{-a}$ are displayed in Fig. 2 and those high-lying isomers are shown in Figs. S3-S4. In $\text{SM}^- \cdot \text{SA}_z\text{-a}$, the SM^- and SA_z fragments interact with each other via three N-H \cdots O HBs, two of which are $\text{SA}_z @ \text{N-H} \cdots \text{O} @ \text{SM}^-$ with the bond lengths of 1.71/1.87 Å, and the third HB of $\text{SM}^- @ \text{N-H} \cdots \text{O} @ \text{SA}_z$ with the bond length of 2.19 Å. Upon photodetachment, the former type of HBs are elongated to 2.14/2.10 Å, while the third HB is shortened to 1.67 Å. In addition, the S-N bond length of SA_z increases from 1.86 Å (LBO of 0.382) to 1.95 Å (LBO of 0.238), but the S-N bond length of SM^- (1.70 Å) remains almost unchanged and the LBO values slightly increase from 0.753 to 0.788.

For the $\text{SM}^- \cdot \text{SA}_c$ type of dimer, the lowest-lying structure of $\text{SM}^- \cdot \text{SA}_c\text{-a}$ possesses an intermolecular HB network consisting of one O-H \cdots O HB and two N-H \cdots O HBs. All high-lying isomers with $\Delta E > 3$ kcal/mol are found to possess only two HBs (Fig. S4). The length of the $\text{SM}^- @ \text{O} \cdots \text{H-O} @ \text{SA}_c$ HB (1.47 Å) is substantially shorter than those of $\text{SM}^- @ \text{O} \cdots \text{H-N} @ \text{SA}_c$ (1.84 Å) and of $\text{SM}^- @ \text{N-H} \cdots \text{O} @ \text{SA}_c$ HB (2.11 Å). After photodetachment, the first two HBs become elongated 1.47/1.84 Å \rightarrow 1.86/2.18 Å, respectively, while the third one is shortened 2.11 \rightarrow 1.82 Å. Meanwhile, the S-N bond lengths in SA_c hardly change (1.66 \rightarrow 1.65 Å) and the corresponding LBO values slightly increase (0.872 \rightarrow 0.930). The S-N bond length in SM^- decreases from 1.70 to 1.62 Å accompanying by a significant increase in LBO value (0.762 \rightarrow 1.044), indicating an enhanced bond covalency during the ionization process.

Notably, dimerization can increase the LBO value and covalent component of the S-N bond, for instance, from SA_z (0.139) to $\text{SA}_z \cdot \text{SA}_z$ (0.280 / 0.266), and from SM^- (0.618) to $\text{SM}^- \cdot \text{SA}_z$ (0.753) / $\text{SM}^- \cdot \text{SA}_c$ (0.762). In contrast, the covalency of the S-N bond in SA_c is relatively insensitive to dimerization (LBOs of 0.928 for SA_c , 0.929 for $\text{SA}_z \cdot \text{SA}_c$ and 0.872 for $\text{SM}^- \cdot \text{SA}_c$). Canonical SA is favored over zwitterionic SA in homodimer clusters, e.g., $\text{SA}_z \cdot \text{SA}_c$ is 2.02 kcal/mol more stable than $\text{SA}_z \cdot \text{SA}_z$ and $\text{SM}^- \cdot \text{SA}_c$ is preferred over $\text{SM}^- \cdot \text{SA}_z$ by 4.71 kcal/mol (Fig. S1). Isomerization conversion from $\text{SM}^- \cdot \text{SA}_c$ to $\text{SM}^- \cdot \text{SA}_z$ needs to overcome a significant barrier of 39.44 kcal/mol (Fig. 3), indicating $\text{SM}^- \cdot \text{SA}_c$ to be dominant in the experiment. In addition, the dynamic conversion process is displayed in the Movie S1 of Supplementary Materials, that involves a rotation of $^5\text{NH}_2$ group in SA_c to reserve a suitable position for the 3rd proton to attack,

This is the author's peer reviewed, accepted manuscript. However, the online version of record will be different from this version once it has been copyedited and typeset.

PLEASE CITE THIS ARTICLE AS DOI: 10.1063/5.0190757

accompanying with two fragments of SM^- and SA_c gradually moving away (I \rightarrow II); a rotation of ${}^2\text{O}-{}^8\text{H}$ to break ${}^2\text{O}-{}^8\text{H}\cdots{}^{10}\text{O}$ HB and induce proton transfer of ${}^8\text{H}$ forming the ${}^5\text{NH}_3$ segment (II \rightarrow III); a further rotation of the ${}^5\text{NH}_3$ group accompanying with the two fragment gradually approaching (III \rightarrow IV); and finally a new ${}^5\text{N}-{}^8\text{H}\cdots{}^{10}\text{O}$ HB formation in $\text{SM}^- \cdot \text{SA}_z$ (IV \rightarrow V).

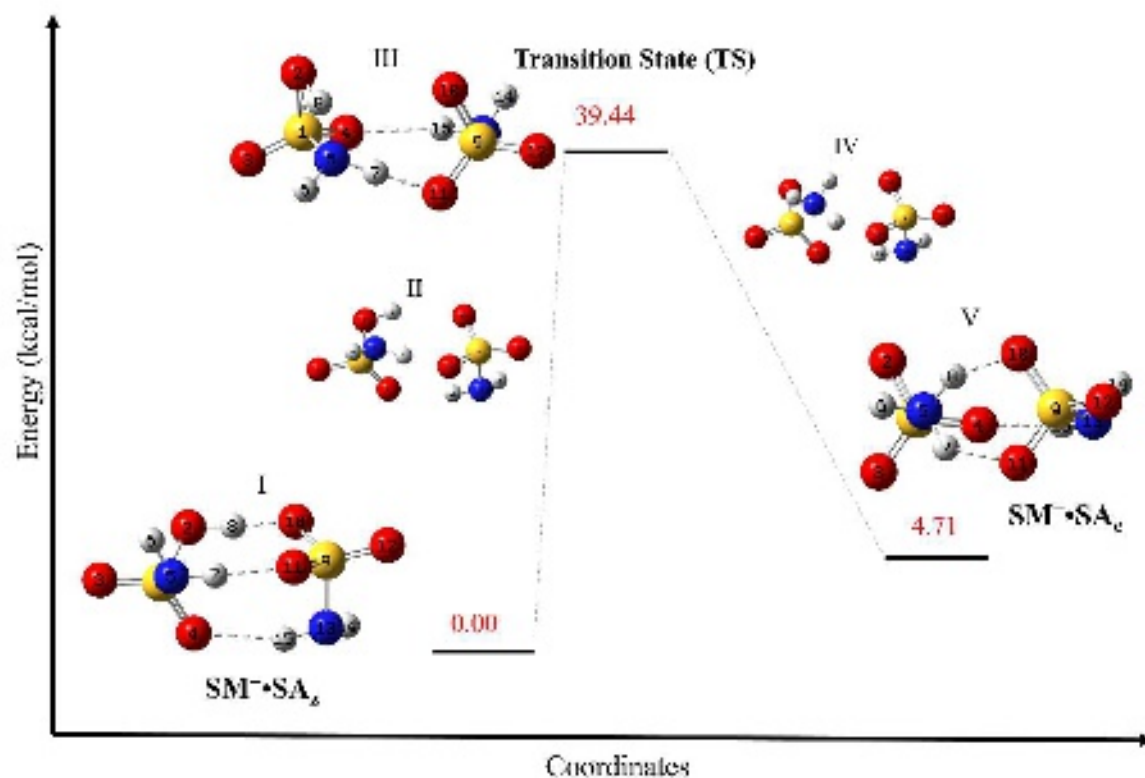


FIG. 3. The transition-state (TS) calculation for the conversion reaction between isomers $\text{SM}^- \cdot \text{SA}_c$ -a and $\text{SM}^- \cdot \text{SA}_z$ -a using intrinsic reaction coordinate (IRC) at the B3LYP-D3(BJ)/aug-cc-pVTZ level with a step-size of 0.005 bohr and the SP energies are refined at the CCSD(T)/aug-cc-pVTZ level. Note that the geometries of II and IV derived from the two side of IRC path are displayed to show the TS evolution, instead of real local minimum (See Movie S1).

B. Calculated VDEs/ADEs and intermolecular BEs

Based on the above optimized structures, the CCSD(T)/aug-cc-pVTZ VDEs and ADEs of SM^- , $\text{SM}^- \cdot \text{SA}_z$, $\text{SM}^- \cdot \text{SA}_c$ and the binding energies (BEs) are calculated (Table I). Compared to the experimental data of SM^- , the absolute deviations (ADs) are 0.04 eV for VDE and 0.05 eV for

ADE. For the dimer anion, the calculated VDEs are quite close and both in excellent agreement with the experimental measurements with ADs less than 0.05 eV. Notably, the predicted ADE of $SM^- \cdot SA_z$ is 0.56 eV smaller compared to the experimental ADE, while the computed ADE of $SM^- \cdot SA_c$ shows a much better agreement with the experimental data with AD \sim 0.22 eV. These SP energy calculations suggest $SM^- \cdot SA_c$ to be dominant in the experiment, a conclusion consistent with the above transition-state calculation analysis.

To evaluate the intermolecular interaction strength of the dimers, the BEs are calculated at the CCSD(T)/aug-cc-pVTZ level (Table I). The calculated BEs for the dimers are in the range of 44 – 49 kcal/mol (1.91 – 2.12 eV). The BE value of $SM^- \cdot SA_c$ is 5 kcal/mol larger than that of $SM^- \cdot SA_z$, indicating a stronger HB interaction in the former. The calculated BEs are slightly larger than the experimental determination (Δ VDE) of 1.56 eV as expected, because the weak intermolecular interactions between two neutral fragments SM^* and SA ($BE_{neutral}$) are not considered in the experimental estimation ($BE = \Delta$ VDE + $BE_{neutral}$).^{21, 43}

C. Molecular orbitals and NPA charge analyses

Based on the generalized Koopmans theorem (GKT)⁴⁴, the density of state (DOS) spectra are simulated, which overall reproduce the experimental NIPE spectra (Fig. 1), albeit that both $SM^- \cdot SA_z$ (in grey) and $SM^- \cdot SA_c$ (in black) predict similar DOS spectra. To reveal the electron ionization behaviors during the photodetaching process, the frontier molecular orbitals (FMOs), Dyson orbitals (DOs) and charge difference $\Delta\rho$ are calculated and displayed in Fig. 4. Complementary to the FMOs, the DOs⁴⁵⁻⁴⁷ further take into account the ionization probability between the source and target states and are calculated by the generalized overlap between the wave functions of anionic state of N+1 electrons and ionized neutral state of N electrons. The DOs are proven to reasonably reflect the position of electron ionization during the ionization process.

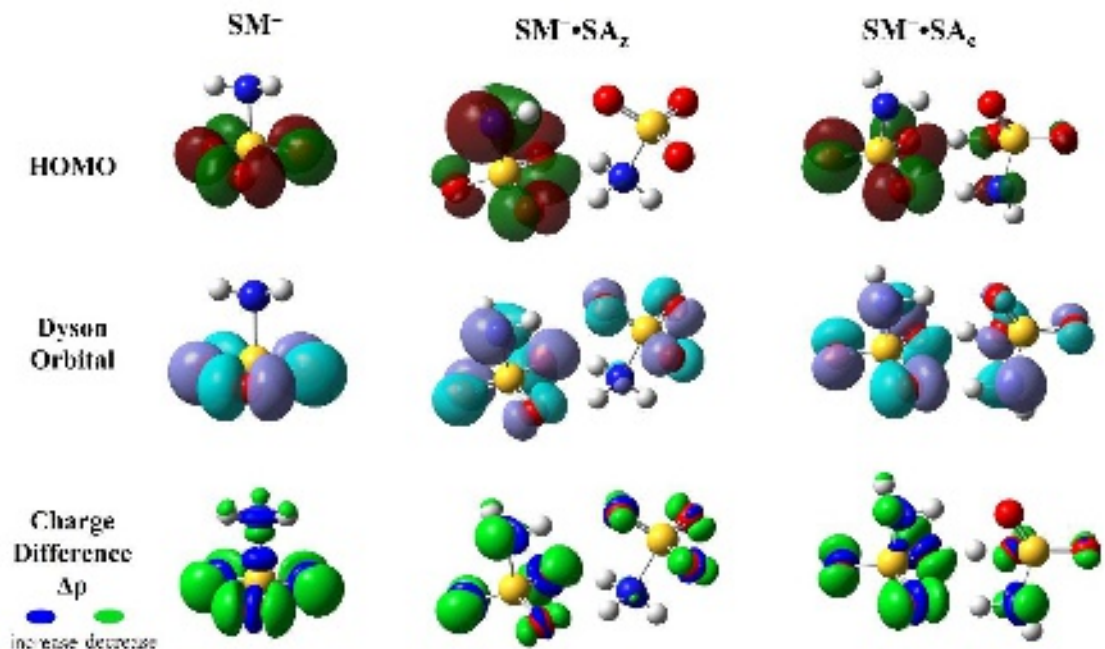


FIG. 4. Plots of highest occupied molecular orbitals (HOMOs) (isovalue = 0.04 a.u.), Dyson orbitals (isovalue = 0.04 a.u.) and charge difference $\Delta\rho$ after ionization (isovalue = 0.004 a.u.) of SM^- , $SM^- \cdot SA_z$, $SM^- \cdot SA_c$ at the B3LYP-D3(BJ)/aug-cc-pVTZ level.

For the $H_2N \cdot SO_3^-$ monomer, detaching one electron from HOMO allows formation of the doublet neutral ground state of $H_2N \cdot SO_3^{\cdot}$. The DO of the monomer consists of three pairs of oxygen lone pair electrons resembling its HOMO distribution. In line with the charge difference $\Delta\rho$ and NPA analysis (Fig. S5), one excess electron mainly detaches from the SO_3 moiety, making it from locally electron-rich (-0.632 e) to electron-deficient ($+0.216$ e). The SO_3 and NH_2 groups contribute -0.848 e and -0.152 e, respectively, to the photodetachment process. For $SM^- \cdot SA_z$ dimer, the simulated DOS spectra indicate the HOMO and HOMO-1 are nearly degenerated with an energy splitting of 0.04 eV. The DO mainly distributes from the $NH_2 \cdot SO_3^-$ (SM^-) fragment consisting of one pair of nitrogen lone pair electrons and three pairs of oxygen lone pair electrons (similar to HOMO), as well as the oxygen lone pair electrons on the ${}^+H_3N \cdot SO_3^-$ (SA_z) fragment. The NPA analysis indicates that the $-SO_3$ / $-NH_2$ groups in SM^- and $-SO_3$ group in SA_z contribute -0.445 e, -0.428 e, -0.126 e, respectively, to the ionization process, suggesting a significant electron donation from $-NH_2$ in SM^- . For the $SM^- \cdot SA_c$ dimer, the HOMO and HOMO-1 are separated with an energy splitting of 0.1 eV. The HOMO is more delocalized with extended distribution on SA_c , that is also reflected by the larger induced charge (-0.142 e of SA_c vs. -0.090

This is the author's peer reviewed, accepted manuscript. However, the online version of record will be different from this version once it has been copyedited and typeset.

PLEASE CITE THIS ARTICLE AS DOI: 10.1063/5.0190757

e of SA_z) (Fig. S5). The DO of $\text{SM}^- \cdot \text{SA}_c$ looks similar to that of $\text{SM}^- \cdot \text{SA}_z$, but with more contribution from the nitrogen lone pair electrons of NH_2 in SA_c . During the photodetachment process, the SO_3 , NH_2 groups of SM^- and SA_c contribute $-0.719 e$, $-0.137 e$, $-0.144 e$, respectively. In short, DO, $\Delta\rho$ and NPA charge analysis suggest that not only the deprotonated $\text{NH}_2 \cdot \text{SO}_3^-$ fragment but also the attached $\text{H}_3\text{N} \cdot \text{SO}_3 / \text{H}_2\text{N} \cdot \text{SO}_2\text{OH}$ molecules participate in the electron ionization process, accompanied by charge transfer (or charge redistribution) between fragments.

TABLE II. The energy decomposition analysis (in kcal/mol) of $\text{SM}^- \cdot \text{SA}_z$ and $\text{SM}^- \cdot \text{SA}_c$ dimers calculated at the $\text{SAPT2+(3)\delta MP2/aug-cc-pVTZ}$, and $\text{sobEDA w-B3LYP-D3(BJ)/6-311+G(2d,p)}$ levels. The contribution percentages of each attraction component are listed in brackets.

SAPT	BE_{total}	E_{elst}	E_{ind}	E_{dis}	E_{exch}
$\text{SM}^- \cdot \text{SA}_z$	44.32	55.39 (63.1%)	19.49 (22.2%)	12.91 (14.7%)	-43.47
$\text{SM}^- \cdot \text{SA}_c$	49.77	62.54 (56.8%)	31.21 (28.3%)	16.39 (14.9%)	-60.38
sobEDA w	BE_{total}	E_{elst}	E_{orb}	E_{dis}	E_{xrep}
$\text{SM}^- \cdot \text{SA}_z$	44.70	55.17 (59.8%)	24.15 (26.2%)	12.99 (14.0%)	-47.61
$\text{SM}^- \cdot \text{SA}_c$	49.68	62.47 (54.5%)	36.91 (32.2%)	15.29 (13.3%)	-64.99

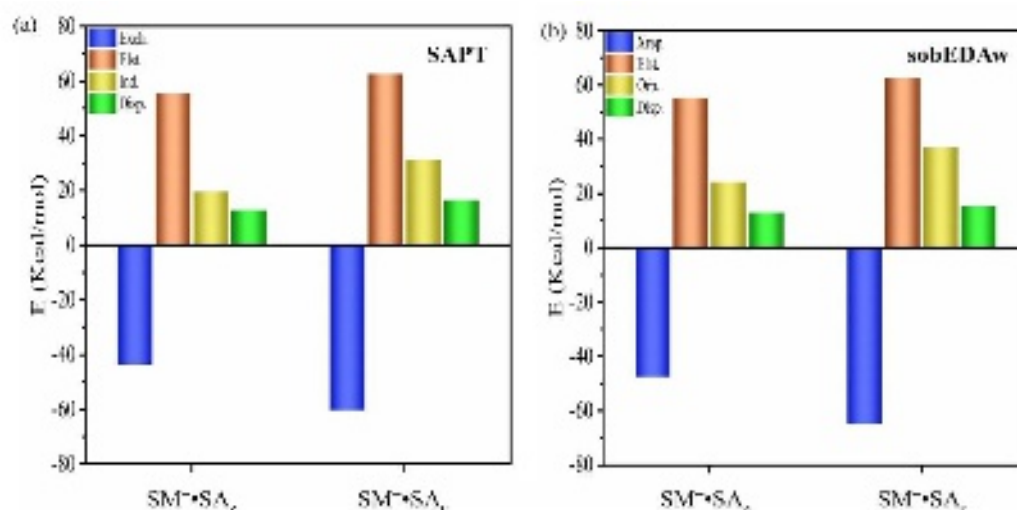


FIG. 5. Components of two different decomposition analyses for $\text{SM}^- \cdot \text{SA}_z$ and $\text{SM}^- \cdot \text{SA}_c$ dimers. (a) Exchange, electrostatic, induction and dispersion terms from SAPT analysis at the $\text{SAPT2+(3)\delta MP2/aug-cc-pVTZ}$ level, and (b) exchange-repulsion, electrostatics, orbital interaction, and dispersion derived from $\text{sobEDA w (B3LYP-D3(BJ)/6-311+G(2d,p))}$ analysis.

D. Energy decomposition analysis of HBs

To further provide in-depth understanding of the nature of intermolecular HB interactions, the energy decomposition analysis (EDA) of HBs in the dimer is performed (see Fig. 5 and Table II). The total interaction energy can be decomposed into four physical terms, which are electrostatic term, exchange term, induction term, and dispersion term (i.e., $E_{tot} = E_{elst} + E_{exch} + E_{ind} + E_{dis}$) based on the SAPT framework. Meanwhile, to allow for a direct comparison, it can be also decomposed into four terms with similar physical meanings, which are electrostatic term, exchange-repulsion term, orbital interaction term, and dispersion term (i.e., $E_{tot} = E_{elst} + E_{xrep} + E_{orb} + E_{dis}$) based on the sobEDA_w method. Note that although different decomposition terms are given, the orbital interaction term E_{orb} provided by the sobEDA_w may be considered qualitatively comparable to the SAPT induction term E_{ind} , and the destabilizing exchange-repulsion term E_{xrep} from the sobEDA_w may be compared with the exchange term E_{exch} provided by the SAPT analysis. The electrostatic term, the orbital interaction (induction) term, and the dispersion term reflect the intermolecular attraction with positive values (Tab. 2), while the exchange-repulsion terms represent the intermolecular repulsion with negative values. Additionally, the contribution percentage of each attractive component in the total attraction energy are listed in brackets, i.e., $[E_i/(E_{elst} + E_{orb/ind} + E_{dis})] \times 100\%$.

First, the attractions of HBs in the dimer are mainly attributed to the classical electrostatic interaction with significant contributions of 55% – 63% for all the isomers, followed by the orbital interaction (or induction) term (22% – 32%), and the dispersion term (13% – 15%). Next, the calculated total BEs based on the SAPT and sobEDA_w approaches agree with each other and are found in excellent agreement with the CCSD(T)-calculated values using counterpoise method (Tab. 1). All the energy differences among the three methods are within 1 kcal/mol for each specific isomer, indicating the reliability of employed methods for BE calculations. Notably, the stronger HB interactions in $SM^- \cdot SA_c$ versus $SM^- \cdot SA_z$ can be attributed to their greater contribution of orbital interaction (32.3% in $SM^- \cdot SA_c$ versus 26.2% in $SM^- \cdot SA_z$) or induction effect in SAPT (28.3% in $SM^- \cdot SA_c$ versus 22.2% in $SM^- \cdot SA_z$). Such a larger orbital interaction or induction contribution in $SM^- \cdot SA_c$ dimer also echoes a larger induced charge distribution on its neutral SA fragment based on the NPA analysis.

This is the author's peer reviewed, accepted manuscript. However, the online version of record will be different from this version once it has been copyedited and typeset.

PLEASE CITE THIS ARTICLE AS DOI: 10.1063/5.0190757

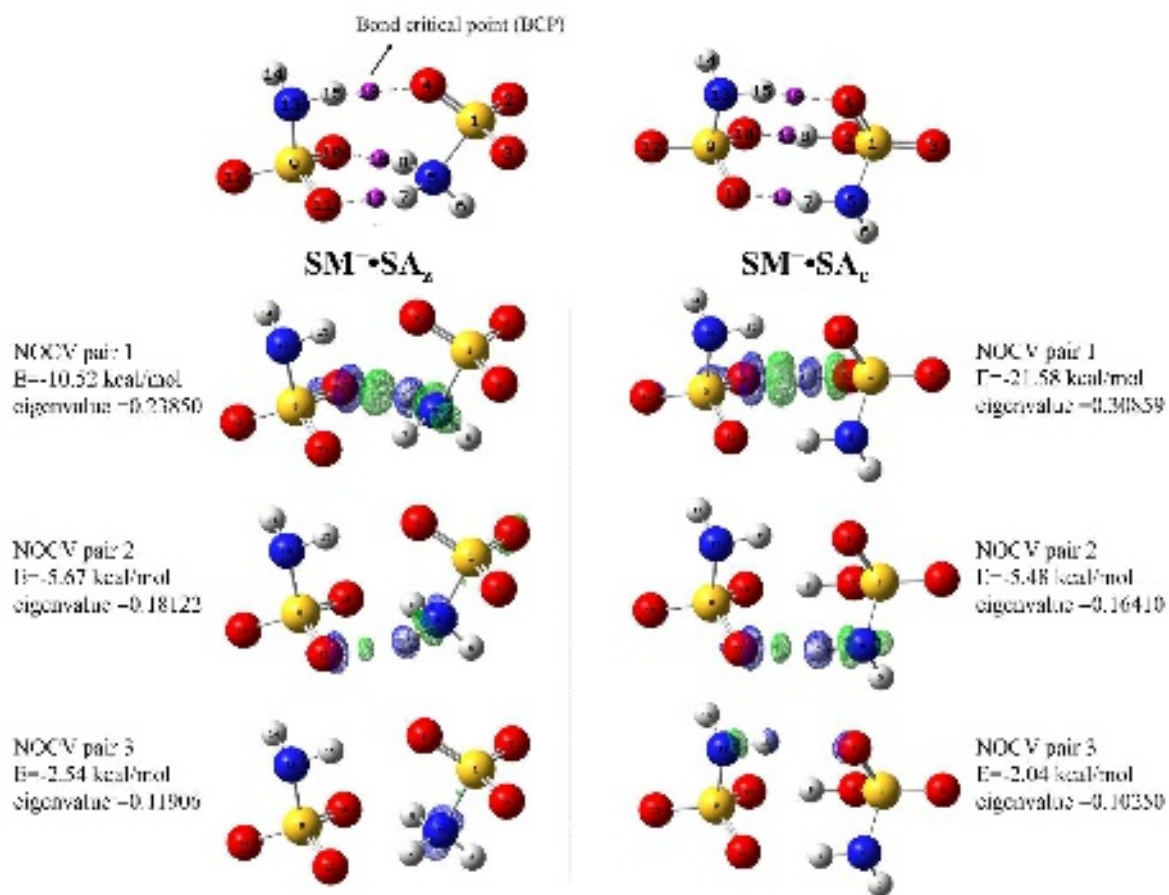


FIG. 6. Schematic diagram of the bond critical points (BCPs) (in purple) of HBs based on AIM theory and ETS-NOCV analysis (isovalue = 0.004 a.u.) of $SM^- \cdot SA_z$ and $SM^- \cdot SA_c$ dimers. The corresponding orbital interaction energies and eigenvalues for each NOCV pair are also listed.

To further analyze each specific HB in $SM^- \cdot SA_z$ and $SM^- \cdot SA_c$, the binding strength of HBs are evaluated based on the atom-in-molecule (AIM)⁴⁸ theory by computing the electron density at the bond critical point (BCP)⁴⁹, ρ_{BCP} . It has been demonstrated by Emamian *et al.* that the HB strength for charged molecular complexes can be quantitatively obtained through the fitted equation of $BE = -332.34 \rho_{BCP} - 1.0661$.⁵⁰ Herein, the BE of each HB in the $SM^- \cdot SA_z$ and $SM^- \cdot SA_c$ dimers were calculated accordingly as listed in Tab. S1. The $SM^- @ ^{13}N-^{15}H \cdots ^4O @ SA$ and $SA @ ^5N-^7H \cdots ^{11}O @ SM^-$ bonds possess similar BEs for the two isomers, being only 1.18 and 0.18 kcal/mol larger in $SM^- \cdot SA_c$, respectively. Therefore, the greater binding strength of $SM^- \cdot SA_c$ should be attributed to the much stronger $^2O-^8H \cdots ^{10}O$ HB, whose BE is 11.43 kcal/mol larger than

the corresponding ${}^5\text{N}-{}^8\text{H}\cdots{}^{10}\text{O}$ HB of $\text{SM}^- \cdot \text{SA}_z$. In addition, the extended transition state-natural orbitals for chemical valence (ETS-NOCV) analysis is carried out to analyze orbital interactions between two fragments. The three dominant NOCV (natural orbitals for chemical valence) pairs are calculated and shown in Fig. 6 and the orbital interaction corresponding to NOCV pair leads to electron transfer from the blue region to the green region. It can be seen that dominant NOCV pairs 1 correspond to the orbital interaction of ${}^5\text{N}-{}^8\text{H}\cdots{}^{10}\text{O}$ HB with a strength of -10.52 kcal/mol in $\text{SM}^- \cdot \text{SA}_z$, and to the orbital interaction of ${}^2\text{O}-{}^8\text{H}\cdots{}^{10}\text{O}$ HB with a stronger strength of -21.58 kcal/mol in $\text{SM}^- \cdot \text{SA}_c$, respectively. The difference of orbital interaction strength (11.06 kcal/mol) based on ETS-NOCV analysis is also in good agreement with the corresponding difference of E_{orb} based on sobEDA_w analysis (12.7 kcal/mol), suggesting the decisive role of the dominant NOCV pair 1 (corresponding to ${}^2\text{O}-{}^8\text{H}\cdots{}^{10}\text{O}$ HB) in enhancing BE of $\text{SM}^- \cdot \text{SA}_c$. Moreover, there is an obvious electron density increasing (green) region between hydrogen and HB acceptor atoms, which reflects that even electrostatic dominated hydrogen bonding is accompanied by certain covalent components to further strengthen such a $\text{O}-\text{H}\cdots\text{O}$ HB.

VI. CONCLUSIONS and OUTLOOKS

We reported a combined NIPES and computational study on the geometric and electronic structures of small deprotonated sulfamic acid (SA) anion clusters, i.e., $\text{H}_2\text{N} \cdot \text{SO}_3^-$ (SM^-) monomer and $\text{SM}^- \cdot \text{SA}$ dimer. Upon the addition of one SA molecule, the VDE and ADE of SM^- monomer increase by 1.56 and 1.29 eV, respectively, suggesting the electronic stability of the dimer is substantially enhanced due to strong intermolecular binding interactions between the two. The calculated VDEs and ADEs are found in good agreement with the experimental data, confirming the identified structures as the most stable ones. Further, the two types of dimers corresponding to SM^- binding to a zwitterionic SA and a canonical SA are identified. The LBO values of the zwitterionic S-N bond increase upon dimerization, while the covalent S-N bond in canonical SA is insensitive to dimerization. Structural optimization and AIM, ETS-NOCV analyses all indicate that $\text{SM}^- \cdot \text{SA}_c$ possesses two $\text{N}-\text{H}\cdots\text{O}$ HBs and one superior $\text{O}-\text{H}\cdots\text{O}$ HB that results in a much stronger binding energy rendering it being an advantageous configuration, while $\text{SM}^- \cdot \text{SA}_z$ dimer has three moderate $\text{N}-\text{H}\cdots\text{O}$ HBs. The energy decomposition analyses by SAPT and sobEDA_w

unravel that the binding strength advantage of $SM^- \cdot SA_c$ over $SM^- \cdot SA_z$ to arise from its stronger orbital interaction (or induction effect) between the two fragments.

Given the prominence of sulfamic acid in the atmosphere and environments, it should be considered as a common precursor molecule along with others such as sulfuric acid, organic acids and sea salt molecules that are responsible for atmospheric nucleation and subsequent aerosol chemistry. The immediate implication of this study suggests that the deprotonated $H_2N \cdot SO_3^-$ anion strongly interact with the acid itself and thus can induce homogeneous nucleation. Moreover, this work provides first experimental evidence that canonical form of sulfamic acid, not the zwitterionic form, is preferred in the cluster growth and initial nucleation process.

SUPPLEMENTARY MATERIAL

The workflow of theoretical calculations; SP energy differences between different tautomer and isomers of the neutral acid, acid dimer and deprotonated dimer in both zwitterionic and canonical forms; LBO values of the monomers and dimers; more optimized low-lying isomers of the dimers; NPA charge populations.

ACKNOWLEDGEMENTS

The work was supported by the National Natural Science Foundation of China (Nos. 12034008, 12274128, 12250003, 12204172 and 11727810), Shanghai Rising-Star Program (No. 21QA1402600), and the Program of Introducing Talents of Discipline to Universities 111 Project (B12024). The NIPES work was supported by the U.S. Department of Energy (DOE), Office of Science, Office of Basic Energy Sciences, Division of Chemical Sciences, Geosciences, and Biosciences, Condensed Phase and Interfacial Molecular Science program, FWP 16248. We acknowledge the ECNU Multifunctional Platform for Innovation (001) and HPC Research Computing Team for providing computational and storage resources and the support of NYU-ECNU Center for Computational Chemistry at NYU Shanghai.

Conflict of Interest

The authors have no conflicts to disclose.

Data Availability

The data that support the findings of this study are available from the corresponding authors upon reasonable request.

References

- ¹ G. A. Benson and W. J. Spillane, "Sulfamic acid and its N-substituted derivatives," *Chem. Rev.* **80**, 151-186 (1980).
- ² W. Spillane and J.-B. Malaubier, "Sulfamic Acid and Its N- and O-Substituted Derivatives," *Chem. Rev.* **114**, 2507-2586 (2014).
- ³ W. J. Spillane and M. R. Walsh, "Synthesis and taste analysis of iminylsulfamates (hydrazonylsulfonates) of N-benzaldehyde, N-acetophenone, N-benzophenone and N-isobutyrophenone," *Food Chem.* **55**, 265-269 (1996).
- ⁴ F. von der Haar, H.-J. Gabius and F. Cramer, "Target directed drug synthesis: The aminoacyl-tRNA Synthetases as possible targets," *Angew. Chem. Int. Ed.* **20**, 217-223 (1981).
- ⁵ S.-O. Zaraei, A. R. Abduelkarem, H. S. Anbar, S. Kobeissi, M. Mohammad, A. Ossama and M. I. El-Gamal, "Sulfamates in drug design and discovery: Pre-clinical and clinical investigations," *Eur. J. Med. Chem.* **179**, 257-271 (2019).
- ⁶ J.-Y. Winum, A. Scozzafava, J.-L. Montero and C. T. Supuran, "Sulfamates and their therapeutic potential," *Med. Res. Rev.* **25**, 186-228 (2005).
- ⁷ E. R. Lovejoy, D. R. Hanson and L. G. Huey, "Kinetics and products of the gas-phase reaction of SO₃ with water," *J. Phys. Chem.* **100**, 19911-19916 (1996).
- ⁸ P. M. Pawlowski, S. R. Okimoto and F.-M. Tao, "Structure and stability of sulfur trioxide–ammonia clusters with water: implications on atmospheric nucleation and condensation," *J. Phys. Chem. A* **107**, 5327-5333 (2003).
- ⁹ G. Shen, M. Suto and L. Lee, "Reaction rate constant of SO₃+NH₃ in the gas phase," *J. Geophys. Res: Atmos.* **95**, 13981-13984 (1990).
- ¹⁰ B. N. Ida, P. S. Fudacz, D. H. Pulsifer and J. M. Standard, "A gas- and condensed-phase density functional study of donor–acceptor complexes of sulfur trioxide," *J. Phys. Chem. A* **110**, 5831-5838 (2006).
- ¹¹ Y. Mo and J. Gao, "Polarization and charge-transfer effects in lewis acid–base complexes," *J. Phys. Chem. A* **105**, 6530-6536 (2001).
- ¹² M. Remko, "Theoretical study of molecular structure and gas-phase acidity of some biologically active sulfonamides," *J. Phys. Chem. A* **107**, 720-725 (2003).
- ¹³ M. W. Wong, K. B. Wiberg and M. J. Frisch, "Solvent effects. 2. Medium effect on the structure, energy, charge density, and vibrational frequencies of sulfamic acid," *J. Am. Chem. Soc.* **114**, 523-529 (1992).

- ¹⁴ M. Canagaratna, J. A. Phillips, H. Goodfriend and K. R. Leopold, "Structure and bonding of the sulfamic acid zwitterion: microwave spectrum of $^+H_3N-SO_3^-$," *J. Am. Chem. Soc.* **118**, 5290-5295 (1996).
- ¹⁵ J. W. Bats, P. Coppens and T. F. Koetzle, "The experimental charge density in sulfur-containing molecules. A study of the deformation electron density in sulfamic acid at 78 K by x-ray and neutron diffraction," *Acta. Crystallogr. B.* **33**, 37-45 (1977).
- ¹⁶ F. A. Kanda and A. J. King, "The crystal structure of sulfamic acid," *J. Am. Chem. Soc.* **73**, 484-487 (1951).
- ¹⁷ M. Pszona, K. Haupa, A. Bil, K. Mierzwicki, Z. Szewczuk and Z. Mielke, "Clustering of sulfamic acid: ESI MS and theoretical study," *J. Mass Spectrom.* **50**, 127-135 (2015).
- ¹⁸ K. Haupa, Z. Szewczuk and Z. Mielke, "Clustering of simple aminosulfonic acids—electrospray ionization mass spectrometric study," *Rapid Commun. Mass Spectrom.* **27**, 1993-1998 (2013).
- ¹⁹ T. I. Yacovitch, N. Heine, C. Brieger, T. Wende, C. Hock, D. M. Neumark and K. R. Asmis, "Communication: Vibrational spectroscopy of atmospherically relevant acid cluster anions: Bisulfate versus nitrate core structures," *J. Chem. Phys.* **136**, 241102 (2012).
- ²⁰ B. R. Bzdek, J. W. DePalma, D. P. Ridge, J. Laskin and M. V. Johnston, "Fragmentation energetics of clusters relevant to atmospheric new particle formation," *J. Am. Chem. Soc.* **135**, 3276-3285 (2013).
- ²¹ X.-B. Wang, "Cluster model studies of anion and molecular specificities via electrospray ionization photoelectron spectroscopy," *J. Phys. Chem. A* **121**, 1389-1401 (2017).
- ²² G.-L. Hou, W. Lin, S. H. M. Deng, J. Zhang, W.-J. Zheng, F. Paesani and X.-B. Wang, "Negative ion photoelectron spectroscopy reveals thermodynamic advantage of organic acids in facilitating formation of bisulfate ion clusters: atmospheric implications," *J. Phys. Chem. Lett.* **4**, 779-785 (2013).
- ²³ X.-B. Wang and L.-S. Wang, "Development of a low-temperature photoelectron spectroscopy instrument using an electrospray ion source and a cryogenically controlled ion trap," *Rev. Sci. Instrum.* **79**, 073108 (2008).
- ²⁴ D. Hanstorp and M. Gustafsson, "Determination of the electron affinity of iodine," *J. Phys. B: At. Mol. Opt.* **25**, 1773 (1992).
- ²⁵ X.-B. Wang, Y. Wang, J. Yang, X.-P. Xing, J. Li and L.-S. Wang, "Evidence of significant covalent bonding in $Au(CN)_2^-$," *J. Am. Chem. Soc.* **131**, 16368-16370 (2009).
- ²⁶ T. Lu, Molclus program, Version 1.12, <http://www.keinsci.com/research/molclus.html> (accessed Mar 1, 2022).
- ²⁷ S. Grimme, C. Bannwarth and P. Shushkov, "A robust and accurate tight-binding quantum chemical method for structures, vibrational frequencies, and noncovalent interactions of large molecular systems parametrized for all spd-block elements ($Z = 1-86$)," *J. Chem. Theory Comput.* **13**, 1989-2009 (2017).
- ²⁸ J. J. Stewart, "Optimization of parameters for semiempirical methods V: modification of NDDO approximations and application to 70 elements," *J. Mol. Model.* **13**, 1173-1213 (2007).
- ²⁹ A. D. Becke, "Density-functional thermochemistry. III. The role of exact exchange," *J. Chem. Phys.* **98** (7), 5648-5652 (1993).
- ³⁰ C. Lee, W. Yang and R. G. Parr, "Development of the Colle-Salvetti correlation-energy formula into a functional of the electron density," *Phys. Rev. B* **37**, 785 (1988).
- ³¹ S. Grimme, S. Ehrlich and L. Goerigk, "Effect of the damping function in dispersion corrected density functional theory," *J. Comput. Chem.* **32**, 1456-1465 (2011).

This is the author's peer reviewed, accepted manuscript. However, the online version of record will be different from this version once it has been copyedited and typeset.

PLEASE CITE THIS ARTICLE AS DOI: 10.1063/5.0190757

- ³² D. E. Woon and T. H. Dunning Jr, "Gaussian basis sets for use in correlated molecular calculations. III. The atoms aluminum through argon," *J. Chem. Phys.* **98**, 1358-1371 (1993).
- ³³ K. Kowalski and P. Piecuch, "The method of moments of coupled-cluster equations and the renormalized CCSD [T], CCSD (T), CCSD (TQ), and CCSDT (Q) approaches," *J. Chem. Phys.* **113**, 18-35 (2000).
- ³⁴ S. F. Boys and F. Bernardi, "The calculation of small molecular interactions by the differences of separate total energies. Some procedures with reduced errors," *Mol. Phys.* **19**, 553-566 (1970).
- ³⁵ T. Lu and F. Chen, "Bond order analysis based on the Laplacian of electron density in fuzzy overlap space," *J. Phys. Chem. A* **117**, 3100-3108 (2013).
- ³⁶ M. P. Mitoraj, A. Michalak and T. Ziegler, "A combined charge and energy decomposition scheme for bond analysis," *J. Chem. Theory Comput.* **5**, 962-975 (2009).
- ³⁷ T. Lu and F. Chen, "Multiwfn: a multifunctional wavefunction analyzer," *J. Comput. Chem.* **33**, 580-592 (2012).
- ³⁸ T. M. Parker, L. A. Burns, R. M. Parrish, A. G. Ryno and C. D. Sherrill, "Levels of symmetry adapted perturbation theory (SAPT). I. Efficiency and performance for interaction energies," *J. Chem. Phys.* **140**, 094106 (2014).
- ³⁹ R. M. Parrish, L. A. Burns, D. G. A. Smith, A. C. Simmonett, A. E. DePrince, E. G. Hohenstein, U. Bozkaya, A. Y. Sokolov, R. Di Remigio, R. M. Richard, J. F. Gonthier, A. M. James, H. R. McAlexander, A. Kumar, M. Saitow, X. Wang, B. P. Pritchard, P. Verma, H. F. Schaefer, K. Patkowski, R. A. King, E. F. Valeev, F. A. Evangelista, J. M. Turney, T. D. Crawford and C. D. Sherrill, "Psi4 1.1: An open-source electronic structure program emphasizing automation, Advanced libraries, and interoperability," *J. Chem. Theory Comput.* **13**, 3185-3197 (2017).
- ⁴⁰ T. Lu and Q. Chen, "Simple, efficient, and universal energy decomposition analysis method based on dispersion-corrected density functional theory," *J. Phys. Chem. A* **127**, 7023-7035 (2023).
- ⁴¹ M. Frisch, G. Trucks, H. Schlegel, G. Scuseria, M. Robb, J. Cheeseman, G. Scalmani, V. Barone, G. Petersson, H. Nakatsuji, et al. Gaussian 16, Revision A. 03, Gaussian, Inc., Wallingford CT (2016).
- ⁴² J. Zhang, B. Zhou, Z.-R. Sun and X.-B. Wang, "Photoelectron spectroscopy and theoretical studies of anion- π interactions: binding strength and anion specificity," *Phys. Chem. Chem. Phys.* **17**, 3131-3141 (2015).
- ⁴³ G.-L. Hou, M. Valiev and X.-B. Wang, "Deprotonated dicarboxylic acid homodimers: Hydrogen bonds and atmospheric implications," *J. Phys. Chem. A* **120**, 2342-2349 (2016).
- ⁴⁴ D. J. Tozer and N. C. Handy, "Improving virtual Kohn-Sham orbitals and eigenvalues: Application to excitation energies and static polarizabilities," *J. Chem. Phys.* **109**, 10180-10189 (1998).
- ⁴⁵ Z. Hu, Z. Sun and H. Sun, "Simulation of negative ion photoelectron spectroscopy using a nuclear ensemble approach: Implications from a nuclear vibration effect," *J. Phys. Chem. A* **125**, 6621-6628 (2021).
- ⁴⁶ C. M. Oana and A. I. Krylov, "Cross sections and photoelectron angular distributions in photodetachment from negative ions using equation-of-motion coupled-cluster Dyson orbitals," *J. Chem. Phys.* **131**, 124114 (2009).
- ⁴⁷ D. G. Truhlar, P. C. Hiberty, S. Shaik, M. S. Gordon and D. Danovich, "Orbitals and the interpretation of photoelectron spectroscopy and (e,2e) ionization experiments," *Angew. Chem. Int. Ed.* **58**, 12332-12338 (2019).

This is the author's peer reviewed, accepted manuscript. However, the online version of record will be different from this version once it has been copyedited and typeset.

PLEASE CITE THIS ARTICLE AS DOI: 10.1063/5.0190757

⁴⁸ R. W. F. Bader, *Atoms in Molecules: A Quantum Theory*. (Oxford University Press, New York, 1990).

⁴⁹ E. Espinosa, E. Molins and C. Lecomte, "Hydrogen bond strengths revealed by topological analyses of experimentally observed electron densities," *Chem. Phys. Lett.* **285**, 170-173 (1998).

⁵⁰ S. Emamian, T. Lu, H. Kruse and H. Emamian, "Exploring nature and predicting strength of hydrogen bonds: A correlation analysis between atoms-in-molecules descriptors, binding energies, and energy components of symmetry-adapted perturbation theory," *J. Comput. Chem.* **40**, 2868-2881 (2019).